AOS Theses

In Search of Mouse Models for Exfoliation Syndrome

RACHEL W. KUCHTEY, SAMUEL INSIGNARES, TZUSHAN S. YANG, AND JOHN KUCHTEY

• PURPOSE: Exfoliation syndrome (XFS) is a systemic connective tissue disorder with elusive pathophysiology. We hypothesize that a mouse model with elastic fiber defects caused by lack of lysyl oxidase like 1 (LOXL1 encoded by *Loxl1*), combined with microfibril deficiency due to *Fbn1* mutation (encoding fibrillin-1, $Fbn1^{C1041G/+}$) will display ocular and systemic phenotypes of XFS.

• METHODS: $Loxl1^{-/-}$ was crossed with $Fbn1^{C1041G/+}$ to create double mutant (dbm) mice. Intraocular pressure (IOP), visual acuity (VA), electroretinogram (ERG), and biometry were characterized in 4 genotypes (wt, $Fbn1^{C1041G/+}$, $Loxl1^{-/-}$, dbm) at 16 weeks of age. Optic nerve (ON) area was measured by ImageJ, and axon counting was achieved by AxonJ. Deep whole-body phenotyping was performed in wt and dbm mice. Two-tailed Student *t* test was used for statistical analysis.

• RESULTS: There was no difference in IOP between the 4 genotypes. VA was significantly reduced only in dbm mice. The majority of biometric parameters showed significant differences in all 3 mutant genotypes compared with wt, and dbm had exacerbated anomalies compared with single mutants. Dbm mice showed reduced retinal function and significantly enlarged ON area compared with wt. Dbm mice exhibited severe systemic phenotypes related to abnormal elastic fibers, such as pelvic organ prolapse and cardiovascular and pulmonary abnormalities.

• CONCLUSIONS: Ocular and systemic findings in dbm mice support functional overlap between fibrillin-1 and LOXL1, 2 prominent components of exfoliation material. Although no elevated IOP or reduction of axon numbers was detected in dbm mice at 16 weeks of age, their reduced retinal function and enlarged ON area indicate early retinal ganglion cell dysfunction. Dbm mice also provide insight on the link between XFS and systemic diseases in humans. NOTE: Publication of this article is sponsored by the American Ophthalmological Society. (Am J Ophthalmol 2024;267: 271–285.

EXFOLIATION GLAUCOMA (XFG) IS THE MOST COMMON form of secondary glaucoma due to exfoliation syndrome (XFS), which is a systemic disease with defective connective tissue.[1] Although all forms of glaucoma may lead to irreversible blindness if not diagnosed and managed properly, XFG is particularly aggressive, often requiring surgical intervention.[2] For all forms of glaucoma, the initial site of damage occurs at the optic nerve head (ONH), leading to apoptosis of retinal ganglion cells (RGCs).[3–6] A major hypothesis of glaucoma pathogenesis is that alterations in the biomechanical properties and tissue remodeling of the ONH, which is rich in elastic fibers and collagens, cause damage of RGC axons as they pass through the lamina cribrosa of the ONH.[7] Deformation of the ONH may induce axon transport deficits[8–10] and eventual degeneration and death of RGCs.

A genetic component of XFS is well recognized. An early study conducted by Allingham and colleagues identified 6 Icelandic families with XFS in 2 generations, in which transmission of the disease to the second generation was through an affected parent, demonstrating that XFS can be genetically inherited.[11] Less than a decade later, in 2007, a landmark genome-wide association study (GWAS) identified genomic variants of *LOXL1* associated with XFS/XFG.[12] Over the ensuing years, the association of *LOXL1* with XFS has been confirmed in many studies across multiple ethnic populations.[13] *LOXL1* encodes one of 5 lysyl oxidase enzymes (LOX and LOXL1-4). The major function of lysyl oxidase-like 1 (LOXL1) is to crosslink elastin, which is a prerequisite for the proper formation and stability of elastic fibers.[14,15]

Although the most prominent features of XFS manifest in the eyes, XFS has been associated with systemic disorders, many of them having a defective connective tissue compo-

AJO.com Supplemental Material available at AJO.com.

Accepted for publication June 12, 2024.

From the Vanderbilt Eye Institute, Department of Ophthalmology and Visual Sciences, Vanderbilt University Medical Center (R.W.K., S.I., J.K.), Nashville, Tennessee; Department of Molecular Physiology and Biophysics, Vanderbilt University (R.W.K.), Nashville, Tennessee; Division of Comparative Medicine, Department of Pathology, Microbiology, and Immunology, Vanderbilt University Medical Center (T.S.Y.), Nashville, Tennessee, USA.

Inquiries to Rachel W. Kuchtey, Vanderbilt Eye Institute, Vanderbilt University Medical Center, Nashville, Tennessee, USA; e-mail: rachel.w.kuchtey@vumc.org

0002-9394/$36.00
https://doi.org/10.1016/j.ajo.2024.06.015

nent, such as pelvic floor organ prolapse (POP).[16–20] Defective LOXL1 could well explain systemic manifestations of XFS. Indeed, similar systemic phenotypes due to abnormal elastic fibers are also found in *loxl1* knockout (*Loxl1*$^{-/-}$) mice.[15,21]

In addition to POP, the association of XFS with cardiovascular diseases has been shown by many studies, although conflicting findings also have been reported.[1,22–24] Mechanistically, the higher prevalence of cardiovascular diseases in XFS patients is plausible as the cardiovascular system is rich in elastic fibers and they play important roles in maintaining the stability and normal function of the cardiovascular system. Mutations in *LOX* were reported in hereditary aortopathy, which is a serious condition that can lead to aortic dissection and sudden death.[25] In addition to *LOX*, mutations in other genes have been discovered causing hereditary aortopathy, one of which is *FBN1*, which encodes fibrillin-1.[26] *FBN1* mutations were first identified in Marfan syndrome (MFS), and subsequently in other MFS-related connective tissue diseases.[27] MFS is a multisystem disease with aortopathy as the most common feature.

A major criterion for diagnosing MFS is ectopia lentis due to abnormal zonules[28] that are predominantly composed of fibrillin-1.[29] LOXL1 was also detected in lens zonules.[30] We have previously characterized the ocular features of mouse models with *Fbn1* and *Loxl1* mutations and discovered that those 2 models share some common features, such as deepening of the anterior chamber, suggesting weakening of lens zonules and enlarged optic nerve cross-sectional areas, which is an underrecognized early glaucoma phenotype.[31,32] Both have proven to be valuable mouse models to study eye diseases; however, the late onset and slower progression limit their use. To overcome this, we created a model with both *Fbn1* and *Loxl1* mutations (*Fbn1*$^{C1041G/+}$; *Loxl1*$^{-/-}$), termed double mutant (dbm). Here we report the exacerbated ocular and systemic features in dbm mice.

METHODS

• **ANIMALS AND GENOTYPING:** All animal studies were performed in accordance with the Association for Research in Vision and Ophthalmology guidelines for the Use of Animals in Ophthalmic and Vision Research and were approved by the Institutional Animal Care and Use Committee of Vanderbilt University Medical Center. *Fbn1*$^{C1041G/+}$ mice (previously referred to as *Fbn1*$^{C1039G/+}$)[33] on the C57BL/6J background were originally purchased from the Jackson Laboratory (stock no. 012885). *Loxl1*$^{-/-}$ mice on a129S1/SvImJ background were obtained from Dr Tiansen Li[15] and backcrossed for 10 generations onto the C57BL/6J background. To produce experimental mice on the C57BL/6J background, male mice heterozygous for the *Fbn1*^{C1041G} allele and heterozygous for the *Loxl1*$^{-}$ allele were paired with female mice wt for *Fbn1* and heterozygous for the *Loxl1*$^{-}$ allele. Animals were housed in a facility operated by the Vanderbilt University Division of Animal Care, with 12/12-hour light-dark cycle and ad libitum access to food and water. All experiments were conducted in 16-week-old mice.

The genotype of each experimental mouse was determined at weaning and confirmed after sacrificing. For *Fbn1* genotyping, we used a protocol described on the Jackson Laboratory website (https://www.jax.org/Protocol?stockNumber=012885&protocolID=28863) in which polymerase chain reaction amplification of DNA extracted from ear punch tissue with primers 10958 (5′-CTC ATC ATT TTT GGC CAG TTG-3′) and primer 10959 (5′-GCA CTT GAT GCA CAT TCA CA-3′) resulted in bands of 164 bp for *wt* and 212 bp for *C1041G* alleles of *Fbn1* (Supplemental Figure S1, A).

For *Loxl1* genotyping, polymerase chain reaction amplification of DNA extracted from ear punch tissue using primers S32 (5′-ACA CGT CGG TGC TGG GAT CA-3′); D5 (5′-CTT TCG TAA ACC AGT ATG AGA ACT ACG ATC-3′); and N5 (5′-CGA GAT CAG CCT CTG TTC CAC-3′) (IDT, Coralville, IA) resulted in bands of ~400 bp for *wt* and ~310 bp for *Loxl1*$^{-}$ alleles (Supplemental Figure S1, B), as previously described.[15] Routine genotyping was performed by a genotyping service (Transnetyx) using proprietary assays that were validated using the polymerase chain reaction protocols described above.

• **IOP MEASUREMENTS:** Mice were anesthetized by isoflurane inhalation (2.5% in oxygen) delivered at 1.5 L/min (Vet Equip). IOP of the right eyes was measured within 2 minutes of loss of consciousness to avoid effects of anesthesia on IOP.[34] In addition, to avoid IOP diurnal variation,[35] all measurements were conducted at the same time of the day (between 3 pm to 5 pm) using TonoLab tonometer (Icare). IOP was calculated as the average of 3 separate IOP determinations, each consisting of the mean of 6 error-free readings.

• **VISUAL ACUITY MEASUREMENTS:** Photopic visual acuity (VA) of mice was assessed by the optomotor response OptoDrum (Stria.Tech). Mice were placed, unrestrained, on an elevated platform surrounded by computer monitors while a striped pattern rotates around the animal, triggering the reflex. A camera above the mouse records the behavior, which is automatically detected and analyzed by OptoDrum software. The stimulus pattern is continuously and automatically adjusted during the experiment to find the animal's visual threshold (cycles/degree).

• **ANTERIOR SEGMENT EXAMINATION:** We performed clinical examination using a portable slitlamp (Kowa SL-17, Torrance, CA) by one of the authors (RWK) masked for mouse genotypes. After pupils were dilated with 1 drop of

tropicamide (1%, Bausch & Lomb) and 1 drop of phenylephrine (2.5%, Paragon Bioteck), anterior segment examination was performed with attention to any corneal abnormalities, ease of pupillary dilation with or without posterior synechia, cataract formation, and exfoliation material on the pupillary margin and anterior lens capsule.

• **SPECTRAL DOMAIN OPTICAL COHERENCE TOMOGRAPHY:** Spectral domain optical coherence tomography (SD-OCT) was carried out as previously described.[36] Briefly, mice were anesthetized with ketamine (100 mg/kg) and xylazine (7 mg/kg), wrapped in gauze and placed in a holder. Eyes were kept moist using lubricant eye drops (Refresh Optive; Allergan). All measurements were obtained with "mouse retina" lens using the BioptigenEnvisu R2200 SD-OCT system for rodents (Leica Microsystems), after pupils were dilated with 1% tropicamide (Bausch & Lomb). Mouse position was adjusted until the appearance of Purkinje lines perpendicular to and parallel to the visual axis and centered on the corneal surface. Images were acquired in a rectangular scan pattern consisting of 100 B-scans, each consisting of 1000 A-scans. Image acquisition was completed before lens opacity or corneal damage appeared due to anesthesia.[37,38]

Central corneal thickness (CCT) was determined by digital caliper. The anterior chamber depth (ACD) was defined as the distance from the central posterior surface of the central cornea to the central anterior surface of the lens. Axial length (AL) measurements were determined by the acquisition of a series of 3 images: (1) a posterior image was used to determine the distance from the outer retinal pigment epithelium to the posterior surface of the lens (vitreous + retina), (2) an anterior image was used to determine the distance from the outer corneal surface to the anterior surface of the lens (CCT + ACD), and (3) an image in which the lens was optically folded in half to determine half of the lens axial diameter (½ lens). AL was defined as equal to (vitreous + retina) + (CCT + ACD) + 2 × ½ lens.

Lens thickness was calculated by ½ lens diameter multiplied by 2. On completion of imaging, the mice were injected with atipamezole (1 mg/kg; Patterson Veterinary) to reverse anesthesia and to prevent xylazine-induced corneal damage.[38]

• **ELECTRORETINOGRAM:** Scotopic electroretinogram (ERG) responses were measured using the Espion system (Diagnosys) as previously reported.[31] After dark adaptation overnight, mice were prepared for recordings under dim red illumination. Mice were anesthetized with ketamine/xylazine/urethane (28/11.2/800 mg/kg), and their eyes dilated with 1 drop of tropicamide (1%, Bausch & Lomb) and 1 drop of phenylephrine (2.5%, Paragon Bioteck). After placing mice under a Ganzfeld dome with a heating pad, gold electrodes were placed on the corneas and ground electrodes placed subcutaneously at the flank. Flash stimuli consisted of flashes of white light of 4-ms duration generated by light-emitting diodes.

Waveforms were recorded in response to flashes ranging in intensity from –5 to 0 log cd·s/m^2, in 1-log increments by averaging responses to multiple consecutive flashes at each intensity. Recordings included a 100-ms prestimulus baseline with data collected up to 500 ms after stimulus onset. Raw data were exported into Excel (Microsoft) for analysis. The pSTR, nSTR, and a-wave amplitudes were determined by the peak or trough to baseline. The b-wave amplitudes were measured from the a-wave trough to the b-wave peak. Response latency was defined as the time interval between stimulus onset and the corresponding peak or trough.

• **OPTIC NERVE EVALUATION:** Immediately after euthanization, mice were cardiac perfused with phosphate-buffered saline (PBS) followed by 4% paraformaldehyde in PBS. Eyes were enucleated and optic nerves cut approximately 1.5 mm from the globe as previously described[31] and postfixed in fixative containing 1% glutaraldehyde and 4% paraformaldehyde in PBS. Optic nerves were transferred to 2% osmium tetroxide in PBS for 1 hour before dehydration and embedding in Epon-812/Araldite resin (Electron Microscopy Sciences), as previously described.[31] Using an ultramicrotome (Leica EM UC7), 1-µm-thick cross sections of optic nerves were cut and stained with paraphenylenediamine, which darkly stains the axoplasm of degenerating axons,[39] and mounted with Permount Mounting Medium (Thermo Fisher Scientific).

Stained optic nerve cross sections were imaged with a 100 × 1.45 NA oil immersion objective on a Nikon inverted light microscope equipped with an SLR DS-Ri2 camera (Nikon). Montage images covering the entire nerve cross-section were assembled using NIS-elements software (Nikon). Optic nerve cross-sectional area ~1.5 mm from the globe, excluding the pia mater, was determined as previously described[31] by drawing a polygon around the nerve using ImageJ (https://imagej.net). The total number of axons was determined using AxonJ, an automated counting plugin for Fiji developed by Zarei and associates.[40]

• **DEEP WHOLE-BODY PHENOTYPING:** We observed early and sudden death of dbm mice at around 16 weeks of age; therefore 16-week-old dbm mice and age-matched wt mice were sacrificed for deep phenotyping. Five wt and 6 dbm mice were necropsied for gross and microscopic examination. Collected tissues (heart, aorta, lung, liver, spleen, kidney, brain, spinal column, skin, pancreas, gastrointestinal tract, reproductive tract, skeletal muscle, adrenal glands, and lymph nodes) were fixed en bloc prior to histology processing, paraffin embedding, sectioning, and routine hematoxylin-eosin staining in the Vanderbilt Translational Pathology Share Resource (TPSR). In addition to hematoxylin-eosin staining, sections of the ascending aorta were stained with Movat histochemical stain to examine elastic fiber morphology.

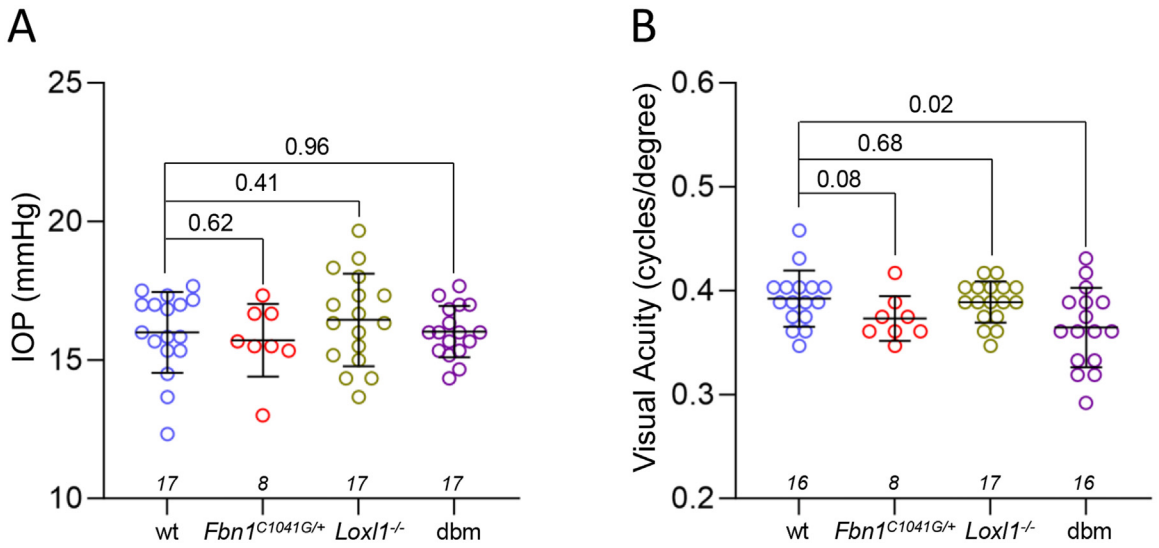

FIGURE 1. Normal IOP but reduced VA in dbm mice. A. At age 16 weeks, there were no differences in IOP compared to wt. No difference of VA was detected in either *Fbn1*$^{C1041G/+}$ or *Loxl1*$^{-/-}$ mice at 16 weeks old compared to wt mice. B. However, the VA in dbm was reduced compared to wt mice. Numbers of mice in each group were indicated above the *x* axis. The *P* values from Student 2-tailed *t* tests for comparisons to wt are indicated above the brackets. Numbers of mice in each group are indicated above the *x* axis. dbm = double mutant, IOP = intraocular pressure, VA = visual acuity, wt = wild type.

• **PERIODIC ACID-SCHIFF STAINING:** Periodic acid-Schiff (PAS) staining has been shown to be capable of recognizing exfoliation material in a previous study[41]; therefore, we chose to use this method to investigate the presence of exfoliation material on the anterior lens capsule. A PAS kit (Sigma; catalog no. 395B) was used following the manufacturer's instruction. Briefly, 7-μm-thick sections were deparaffinized in xylene and rehydrated in deionized water. Slides were immersed in periodic acid solution for 5 minutes at room temperature, rinsed with distilled water, then immersed in Schiff reagent for 15 minutes at room temperature and washed in running tap water for 5 minutes. Sections were counterstained with Gill no. 3 hematoxylin solution for 90 seconds and rinsed in running tap water. Finally, sections were dehydrated in gradient ethanol and mounted using Permount mounting media. Brightfield images were acquired using a microscope equipped with a 20× objective (Nikon).

• **STATISTICAL ANALYSIS:** All experiments were carried out by masked observers. All data are presented as mean ± SD. Graphs were made and statistical analyses were performed using GraphPad Prism version 9.0 (GraphPad Software). Data were analyzed using Student 2-tailed *t* test as indicated in the figure legends. We defined statistical significance as $P \leq .05$. Number of measurements and specific *P* values are indicated in the results or figure legends.

RESULTS

• **DBM MICE DO NOT HAVE ELEVATED IOP:** We previously reported 1-year-old *Loxl1*$^{-/-}$ nonanesthetized mice did not have elevated IOP.[32] Similarly, we did not observe elevated IOP in *Fbn1*$^{C1041G/+}$ mice when compared with wt mice at 1 year of age (data not shown). Not surprisingly, at 16 weeks of age, as shown in Figure 1A, no elevated IOP was detected in *Fbn1*$^{C1041G/+}$, *Loxl1*$^{-/-}$, or dbm mice compared with age-matched wt mice.

• **DBM MICE HAVE REDUCED VISUAL ACUITY:** As shown in our previous publication, 1-year-old *Loxl1*$^{-/-}$ mice showed decreased VA compared with age-matched wt mice.[32] We also reported decreased VA in mice carrying the *Tsk* mutation of *Fbn1* (*Fbn1*$^{Tsk/+}$) at the advanced age of 16 months, although not at 6 months of age.[31] At age 16 weeks, we did not detect VA changes in either *Fbn1*$^{C1041G/+}$or *Loxl1*$^{-/-}$ mice as expected. However, as shown in Figure 1B, we observed significantly reduced VA in 16-week-old dbm when compared with age-matched wt mice.

• **DBM MICE DO NOT HAVE DETECTABLE EXFOLIATION MATERIAL OR CATARACT FORMATION:** Slitlamp examination was performed to check for the presence of exfoliation material and to explore the etiology of reduced VA in dbm mice at 16 weeks of age. We did not observe any exfoliation material either on the pupillary margin or anterior lens capsule. All mice experienced equal dilation of

the pupils without any evidence of posterior synechia formation. We carefully examined the lens and detected no visible cataract formation in any of the mice, regardless of their genotypes. We did not observe the presence of exfoliation material after staining the anterior lens capsule with PAS.

• **EXACERBATED OCULAR BIOMETRIC CHANGES INDUCED BY *FBN1* AND *LOXL1* MUTATIONS:** Thin cornea is a common ocular feature of Marfan patients.[42] In addition, thin cornea was observed in embryos of Marfan mice.[43] We previously reported reduced CCT of *Loxl1*$^{-/-}$ mice at age 1 year.[32] We also reported thinning of CCT of *Fbn1*$^{Tsk/+}$ mice, which was detectable as early as age 3 months and persistent up to age 9 months.[31] Taken together, it was not surprising that we observed by SD-OCT significant thinning of CCT in both *Fbn1*$^{C1041G/+}$ and *Loxl1*$^{-/-}$ mice at age 16 weeks when compared with wt mice. More significantly, dbm mice showed even thinner CCT compared with wt and each single mutant mice (Figure 2, A and 2B).

Similar to CCT, we also observed by SD-OCT other significant biometric changes in dbm mice. The most notable finding was the significant deepening of ACD in dbm mice compared with wt as well as single mutant mice (Figure 2, A and C). We also noticed significantly deeper ACD in *Loxl1*$^{-/-}$ mice compared with wt, but the deepening of ACD in *Fbn1*$^{C1041G/+}$ mice did not reach statistical significance, which could be explained by the mild nature of MFS because of the C1041G mutation and young age.

However, the ACD of dbm was markedly deepened when compared with wt as well as single mutant mice. This is not due to the lens thickness, as we did not observe any significant differences among all 4 genotypes as shown in Figure 2, D. No significant elongation of the eye was observed in mild Marfan *Fbn1*$^{C1041G/+}$ mice, but longer AL was seen in both *Loxl1*$^{-/-}$ and dbm when compared to wt mice, although the difference between *Loxl1*$^{-/-}$ and dbm was not significant (Figure 2, E).

• **RETINAL FUNCTION IS REDUCED IN DBM MICE:** Retinal function measured by ERG, particularly pSTR component, has been widely used to assess RGC function in rodent glaucoma models as shown previously by us and others.[31,44,45] As shown in Figure 3, F, we detected significantly prolonged latency of scotopic threshold response in dbm when compared with wt mice, whereas no difference was detected between *Fbn1*$^{C1041G/+}$ and wt or between *Loxl1*$^{-/-}$ and wt mice at 16 weeks of age. Similarly, as indicated by the average waveform of each genotype, reduced peak of scotopic threshold response in dbm was observed as shown in Figure 3, A through D, although when compared with wt, such reduction was only trending significant. No reduction of response peak was observed in either *Fbn1*$^{C1041G/+}$ or *Loxl1*$^{-/-}$ mice.

TABLE. 1. Incidence of Pelvic Organ Prolapse in dbm Mice

No. of mice	25
No. (%) of mice with POP	11 (44%)
No. of male mice	12
No. (%) of male mice with POP	4 (33%)
No. of female mice	13
No. (%) of female mice with POP	7 (54%)

dbm = double mutant; POP = pelvic organ prolapse.

• **DBM MICE HAVE ENLARGED OPTIC NERVE WITHOUT AXONAL LOSS:** We and others have observed enlarged optic nerve cross-sectional area preceding reduced RGC function and axon numbers in rodent glaucoma models.[46–48] We reported enlarged optic nerve cross-sectional area in 1-year-old *Loxl1*$^{-/-}$ mice.[32] We also previously observed the same phenotype in *Fbn1*$^{Tsk/+}$ mice at age 6 months and persisted to age 16 months.[31] At 16 weeks of age, as shown in Figure 4, there was significant enlargement of optic nerve cross-sectional area in both *Loxl1*$^{-/-}$ and dbm mice when compared to wt.

We were not surprised that there was no significant difference between wt and *Fbn1*$^{C1041G/+}$ mice, as these *Fbn1*$^{C1041G/+}$ mice have overall mild phenotypes. We also compared *Loxl1*$^{-/-}$ and dbm mice and did not observe any significant difference between those 2 groups, indicating that the enlarged optic nerve phenotype in dbm is driven by the *Loxl1*$^{-/-}$ allele. We also performed axon counting using AxonJ in wt and dbm mice. There was no difference between wt and dbm at age 16 weeks (data not shown).

• **LIFE SPAN IS REDUCED IN DBM:** Both *Fbn1*$^{C1041G/+}$ and *Loxl1*$^{-/-}$ mice have relatively normal life span, up to age 2 years. However, dbm mice died much younger, starting at about 12 weeks of age. The survival rate dropped to approximately 80% at 16 weeks. Based on these observations, we chose 16 weeks of age for all experiments reported here.

• **POP WAS FREQUENTLY OBSERVED IN DBM MICE:** One of the phenotypes of *Loxl1*$^{-/-}$ mice is POP, as reported in the original publication.[15] We observed that 44% dbm mice experienced POP within their life span as shown in Table 1. The percentage of POP in female mice was higher than that in male mice (54% vs 33%). We did not observe any wt mice with POP at this age.

• **DBM MICE HAVE DISORDERS IN CARDIOVASCULAR AND PULMONARY SYSTEMS:** The early death in dbm mice prompted us to perform necropsy. As aortic dissection is a common cause of sudden death in patients with MFS,[26] we expected to see hemothorax in dbm mice. Interestingly, we

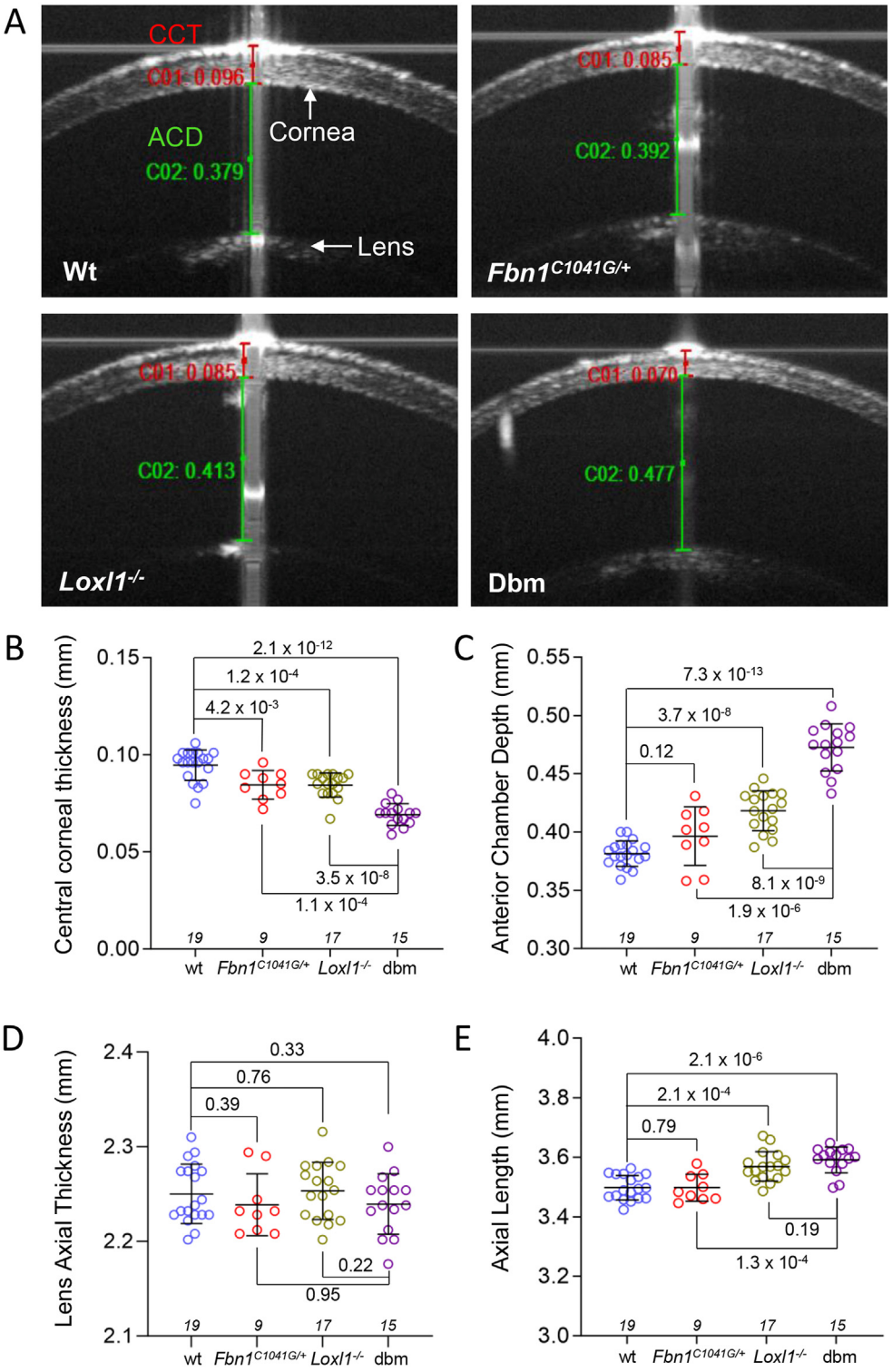

FIGURE 2. Biometric changes in mutant mice. The majority of biometric parameters showed significant differences in all 3 mutant genotypes compared to wt, with exacerbated anomalies found in dbm. Representative OCT images of CCT and ACD measurements in the 4 genotypes, each genotype labeled in lower left corner (A). Thinning of CCT and deepening of ACD in the 3 mutant lines can be appreciated here using wt as a reference. The significant differences of CCT are shown in panel B. Significant deepening of ACD is shown in panel C. No difference of lens thickness was seen among the 4 genotypes (D), and mild elongation of axial length was seen in *Loxl1*$^{-/-}$ and dbm when compared with wt mice (E). The *P* values are shown above or below the brackets indicating comparisons (B, C, D, and E). Numbers of mice in each group are indicated above the *x* axis (B, C, D, and E). ACD = anterior chamber depth, CCT = central corneal thickness, dbm = double mutant, OCT = optical coherence tomography.

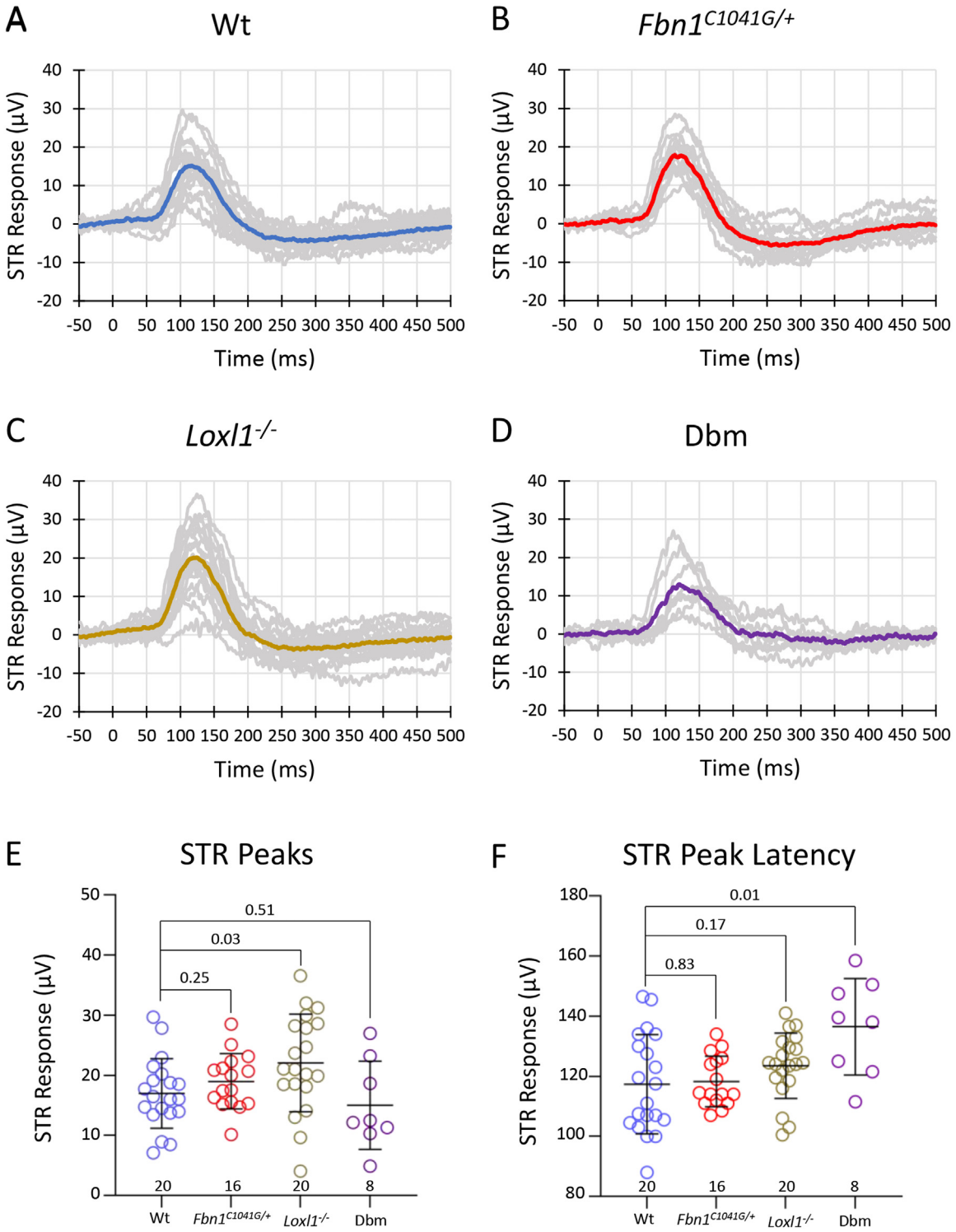

FIGURE 3. Prolonged latency of scotopic threshold response of electroretinography in dbm mice. A-D. Raw waveforms of each individual eye of mice with 4 genotypes are indicated in gray, and colored waveform represents average of all eyes of mice with 4 genotypes. E. There is trend of reduced peak response in dbm mice, but not statistically significant when compared with wt. F. There is prolonged latency in dbm when compared with wt. The *P* values are indicated above the brackets and Numbers of eyes in each group are indicated above the *x* axis. dbm = double mutant,

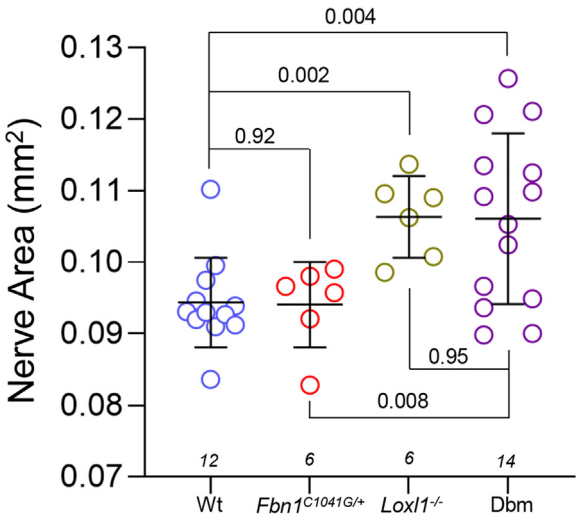

FIGURE 4. Enlarged optic nerve in dbm mice. When compared with wt, dbm mice showed significantly increased optic nerve area (2-tailed Student *t* test, $P = .012$). Similar phenotype was observed in *Loxl1*$^{-/-}$ mice when compared with wt, whereas there was no significant difference between *Fbn1*$^{C1041G/+}$ and wt mice. Comparison between *Loxl1*$^{-/-}$ and wt mice showed no significant difference. The *P* values are indicated above and below the brackets and numbers of eyes in each group are indicated above the *x* axis. dbm = double mutant, , wt = wild type.

instead observed cardiomegaly without obvious hemothorax. This further prompted us to perform thorough gross and histologic deep phenotyping of dbm mice. As shown in Figure 5C, we observed markedly dilated atria and ascending aorta in dbm mice.

Although we did not observe gross body size abnormalities, we measured the tibia length, which revealed no difference between wt and dbm mice (data not shown). Using tibia length for normalization, the heart weight in dbm was significantly greater than wt as shown in Figure 5, A. In addition, the width of the ascending aorta of dbm was significantly increased compared with wt (Figure 5, B). Movat Pentachrome histochemical staining of the ascending aorta showed thinning and fragmented elastic fibers in dbm mice (Figure 5, D).

Although the histologic findings of aortic wall are typical of MFS with aneurism, we suspected other causes of sudden death in dbm mice. Hematoxylin-eosin staining of the heart revealed myxomatous valvular degeneration of both atrioventricular (AV) valves in dbm mice as shown in Figure 6. Both mitral and tricuspid valve leaflets are elongated with irregular and segmental thickening of the spongiosa in dbm mice. The valvulopathy and associated cardiac chamber enlargement likely contributes to early death in dbm mice.

In addition, as shown in Figure 7, severe pulmonary emphysema and bronchiectasis were detected in dbm mice with abundant evidence of diffusely dilated alveoli and bronchioles. We also observed multifocal leukocytoclastic arteritis in the abdominal aorta, peripheral muscular arteries, and aortic root as shown in Supplemental Figure 2.

DISCUSSION

The discovery of genomic variants of *LOXL1* associated with XFS by GWAS[12] has been replicated by many studies, including the largest GWAS using geographically comprehensive samples with diverse populations.[13] However, the *LOXL1* allele flip phenomenon was also well recognized, indicating abnormal LOXL1 is necessary for XFS development, but not sufficient, suggesting that additional factors are needed.[49] We hypothesize that one of the additional factors could be fibrillin-1, which is a key component of microfibril scaffold for elastin deposition and formation of stable elastic fibers.[50,51]

The interaction between fibrillin-1 and LOXL1 has been shown outside the eye. In a study by Busnadiego and associates, when *Fbn1*$^{C1041G/+}$ mice were challenged with β-aminopropionitrile (BAPN), which inhibits all lysyl oxidases, mice with mild MFS developed accelerated aortopathy, including ascending aorta dilation with increased aortic wall elastic fiber fragmentation resulting in early death.[52] Within the eye, we used the same protocol as Busnadiego and associates to treat *Fbn1*$^{C1041G/+}$ mice with BAPN to test if double hits with both fibrillin-1 and LOX defects will worsen the ocular phenotypes.

We discovered that inhibition of entire LOX family proteins indeed enhanced optic nerve expansion in *Fbn1*$^{C1041G/+}$ mice.[53] Although in that study, the entire LOX family (LOX, LOXL1-4) was inhibited by BAPN, it lends support for overlapping and, possibly, interacting roles of fibrillin-1 and LOXL1. In terms of their roles within the eye, specifically related to XFS, LOXL1 and fibrillin-1 are 2 major components of exfoliation material.[54] In addition, using human samples, Schlötzer-Schrehardt demonstrated reduced expression of LOXL1 and fibrillin-1 in the lamina cribrosa of XFS and XFG patients.[55] To focus on interaction specifically between LOXL1 and fibrillin-1, we created our unique dbm mouse model with haploinsufficiency C1041G mutation of *Fbn1* and knockout of *Loxl1* allele to investigate ocular and systemic manifestations by deep phenotyping and in-depth ocular structural and functional analyses.

We first investigated biometric features of dbm mice and compared them with wt, *Fbn1*$^{C1041G/+}$, and *Loxl1*$^{-/-}$ mice at age 16 weeks. We detected thinning of CCT of dbm mice. We previously reported ocular findings of mice carrying a different *Fbn1* mutation (*Fbn1*$^{Tsk/+}$).[46] The systemic phenotypes of *Fbn1*$^{Tsk/+}$ mice include thickened skin and visceral fibrosis.[56] In the eyes, we discovered that they have thin CCT, which could be detected as early as 3 months of age. This phenotype likely occurred earlier, as we observed

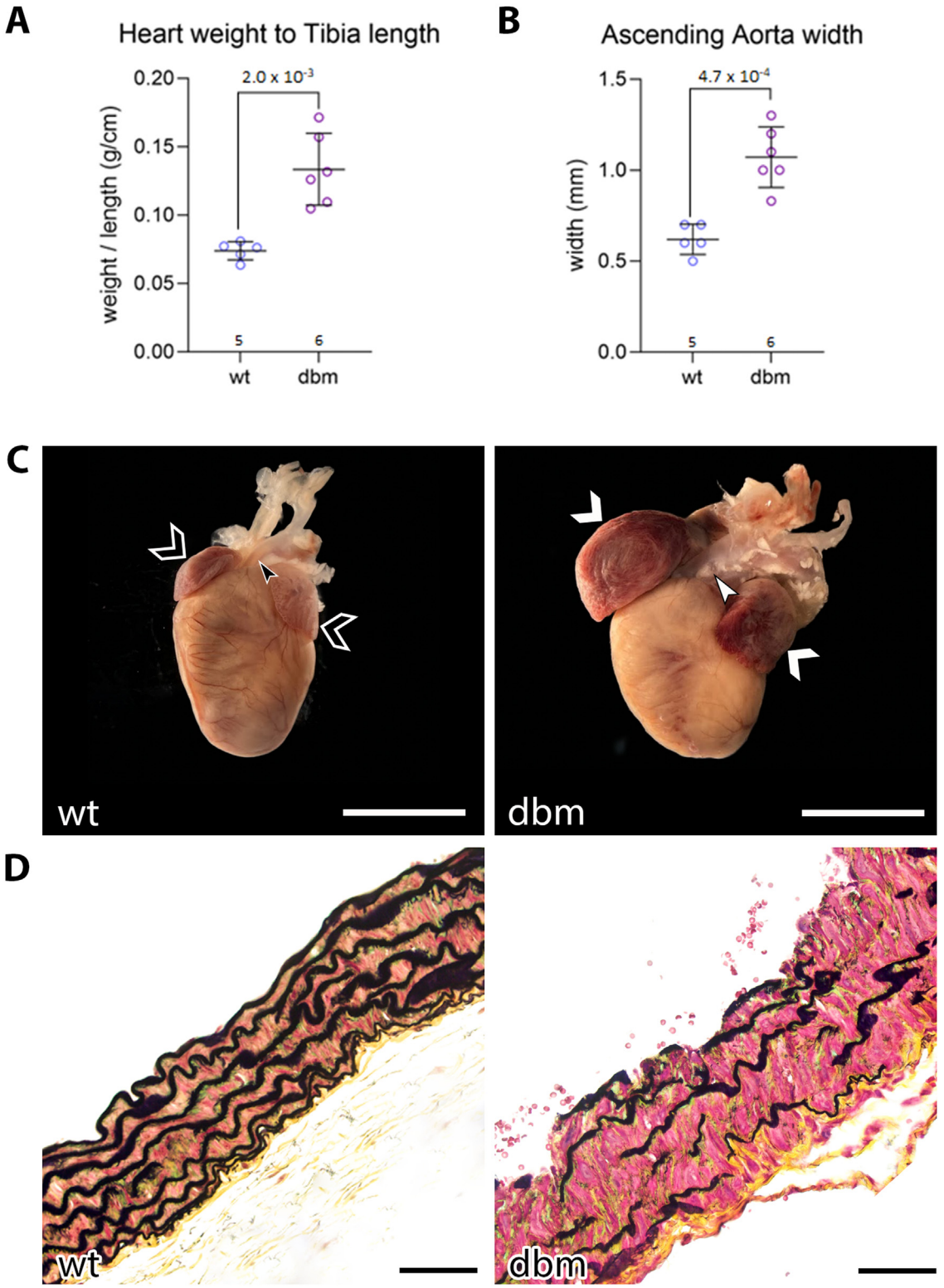

FIGURE 5. Enlarged heart and aorta phenotype of dbm compared with wt mice. A. Significant cardiomegaly was observed in dbm compared with wt mice. B. The ascending aorta width of dbm was also significantly dilated compared with wt mice. Gross comparison of hearts from wt and dbm mice showing both right and left atria (chevrons) were markedly dilated, and the ascending aorta (arrowheads) was visibly wider in dbm hearts (scale bar = 5 mm). Movat Pentachrome histochemical staining of the ascending aorta showed linear and continuous elastic fibers in wt. In contrast, the elastic fibers are thin, fragmented, and discontinuous in dbm mice (D) (scale bar = 50 μm). dbm = double mutant, , wt = wild type.

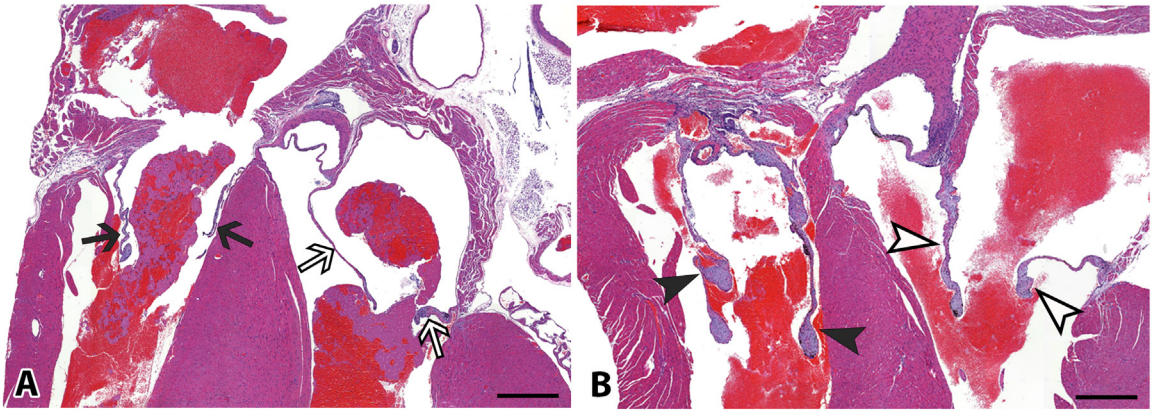

FIGURE 6. Myxomatous valvular degeneration of both atrioventricular (AV) valves in dbm mouse hearts. Hematoxylin-eosin staining of wt mouse heart showed consistently smooth and thin tricuspid and mitral valves (A). Both AV valve leaflets are elongated with irregular and segmental thickening of the spongiosa (B). (tricuspid valve: black arrowheads; mitral valve: white arrowheads). Scale bar = 500 μm. dbm = double mutant, , wt = wild type.

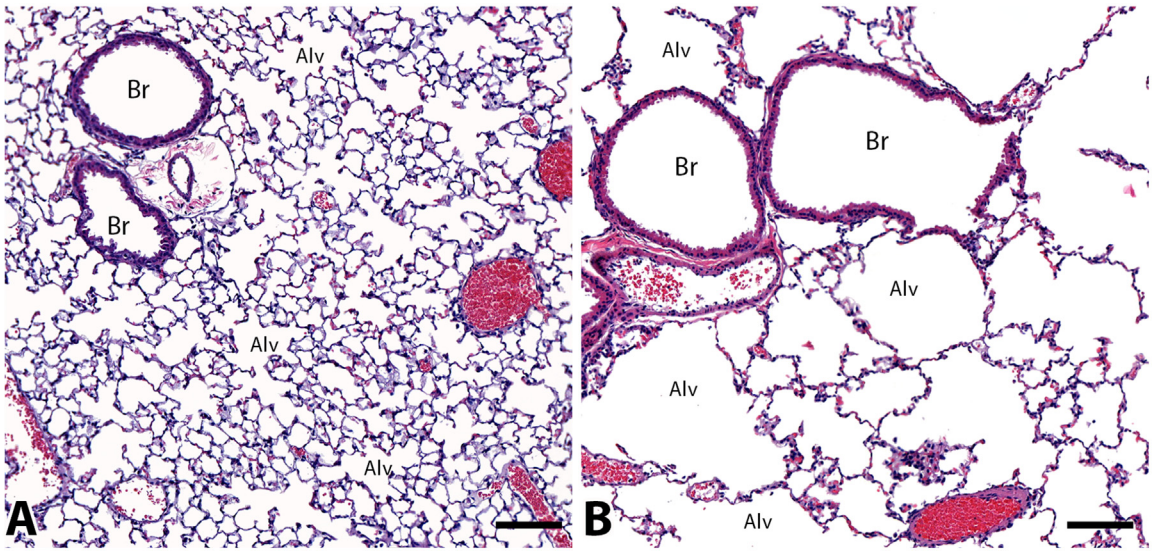

FIGURE 7. Pulmonary emphysema and bronchiectasis in dbm mouse lungs. Lung section from wt mice showed normal bronchioles (Br) and alveoli (Alv) (A), whereas dbm mouse lungs had diffusely dilated alveoli and bronchioles (B). Scale bar = 100 μm. dbm = double mutant, wt = wild type.

the persistent but nonprogressive nature of thin CCT in *Fbn1*$^{Tsk/+}$ mice up to 9 months of age.

Corneal thinning is a common ocular phenotype of Marfan syndrome in human patients.[57] When comparing adult with pediatric MFS patients, Suwal and associates did not detect significant difference between them, indicating the nonprogressive nature of thin CCT.[58] Research led by Meek using a different Marfan mouse model revealed thinning of CCT detectable from the embryonic stage to an adulthood of age 3 months.[43,59] Although the *Fbn1*$^{C1041G/+}$ Marfan mouse model reported here is considered a mild Marfan model because of its mild and late onset of cardiovascular phenotypes,[33] we were not surprised to see the thinning of CCT of *Fbn1*$^{C1041G/+}$ mice at 16 weeks of age, and we speculate this was congenital.

It is worth noting that *FBN1* has been associated with central corneal thickness, a known risk factor for primary open angle glaucoma in a cross-ancestry GWAS study[60] as well as in a large Australian population study.[61] Similarly, we reported thinning of CCT in *Loxl1*$^{-/-}$ mice at 1 year of age.[32] In this study, in line with previous findings, we observed thinning of CCT in both *Fbn1*$^{C1041G/+}$ and *Loxl1*$^{-/-}$

mice at age 16 weeks. Fibrillin-1 and all 5 LOX family members are present in the cornea, and *LOX* mutations have been found in keratoconus patients,[62,63] although the role of LOXL1 in keratoconus is less clear. Intriguingly, we observed exacerbated thinning of CCT in dbm mice when compared to each single mutant genotype (Figure 2, B), indicating interaction of fibrillin-1 and LOXL1 within the eye.

In addition to thin corneas, one of the key findings of Marfan syndrome is progressive ectopia lentis due to weakened zonular fibers, which are largely composed of fibrillin-1 protein.[57] Because it is challenging to detect ectopia lentis in mice by slitlamp examination, even at advanced stages, we used SD-OCT to measure the ACD. As shown in Supplemental Figure S3, we detected extreme deepening of the ACD in $Fbn1^{Tsk/+}$ mice at advanced age likely due to posterior movement of lens caused by abnormal zonular fibers. This lends support for using SD-OCT measurement of ACD as a surrogate of zonule stability.

We did not observe deepening of ACD in $Fbn1^{C1041G/+}$ mice at age 16 weeks, which was consistent with the mild nature of the C1041G mutation of *Fbn1* in terms of MFS phenotypes and the progressive nature of ectopia lentis in MFS. We did observe deepening of the ACD in $Loxl1^{-/-}$ mice, which recapitulate some XFS phenotypes, because dislocated lens due to zonular fiber defects is a common phenotype of XFS.[1] Using the same $Loxl1^{-/-}$ mice but at older age (1 year), Wiggs and associates reported a number of ocular features resembling XFS in human patients, such as cataract formation and blood–aqueous barrier breakdown.[64]

Although the biometric phenotypes observed by us here as well as ocular phenotypes reported by Wiggs and associates are mild, the deepening of ACD in $Loxl1^{-/-}$ mice at 16 weeks of age is consistent with an XFS phenotype. More significantly, similar to CCT, we observed exacerbated deepening of ACD in dbm mice, further supporting the interactions between fibrillin-1 and LOXL1. It is interesting to note that the key function of LOXL1 is crosslinking tropoelastin to elastin for stable elastic fiber formation.[65] Lens zonules are composed of elastin-free microfibrils,[29] yet LOXL1 protein was detected in human and bovine zonules,[30] raising the possibility of LOXL1 acting on fibrillin-1, in addition to crosslinking elastin.

We also detected reduced VA in dbm mice. Although the reduction of VA was mild in dbm, this was not observed in $Fbn1^{C1041G/+}$ or $Loxl1^{-/-}$ mice. Although the reduced VA could simply be due to refractive error from biometric changes in dbm mice, it could also be due to reduced retinal function as shown in Figure 3. The enlarged optic nerve phenotype of dbm mice as shown in Figure 5 further supports this possibility. Although reduced VA generally occurs much later in human glaucoma patients, we cannot rule out the possibility of reduced VA in dbm mice related to glaucoma. Interestingly, the dbm mice did not exhibit elevated IOP as shown in Figure 1, A.

It is well established that CCT affects IOP measurement in humans[66]; however, we do not believe normal IOP in all 3 mutant genotypes was influenced by thin CCT of those mice, as we previously demonstrated.[46] This promotes the notion that the reduced retinal function and enlarged optic nerve phenotypes are independent of IOP. It has been recognized that XFG occurs in some patients without elevated IOP.[67,68] The observation of reduced fibrillin-1 and LOXL1 expression in the lamina cribrosa of patients with both XFS and XFG reported by Schlötzer-Schrehardt and associates supports the significant contribution of optic nerve head structure in XFG pathogenesis.[55]

We observed a series of systemic findings through deep phenotyping of dbm mice. The dbm mice sustained early mortality ranging from 12 to 16 weeks of age. This is consistent with increased mortality in BAPN-treated $Fbn1^{C1041G/+}$ mice attributed to exacerbated dilated aorta.[52] The early death of dbm mice prompted us to perform necropsy initially, which revealed cardiomegaly with severe bilateral atrial enlargement. This observation led us to deep phenotyping of dbm mice at age 16 weeks that revealed cardiomegaly, aortic dilation, and valvulopathy in dbm mice. These findings suggest the early death of the dbm may be largely attributed to these cardiac changes and potentially leading to congestive heart failure or fatal cardiac arrythmia. Further investigations likely will shed more light on the observation of XFS associated with atrial fibrillation in humans.[20]

The diagnosis of XFS is through the readily detectable exfoliation material in the anterior segment of the eye. The discovery of exfoliation material elsewhere in the body confirms the systemic manifestations of XFS,[69] although the existing data in the literature on the association with systemic diseases, especially cardiovascular disorders, remain controversial. Using a large electronic medical records database of Maccabi Health Services, Zehavi-Dorin and associates found that among individuals with XFS, the risk of cardiovascular diseases, including hypertension, myocardial infarction, and congestive heart failure, was significantly higher than the control group.[70]

The Blue Mountain Eye Study showed that XFS was associated with a history of angina or hypertension or a combined history of angina, acute myocardial infarction, or stroke.[71] In another study, in addition to confirming an increased risk of respiratory, cardiovascular, and urogenital comorbidities, Scharfenberg and associates found an increased risk of cardiac valve disorders among XFS patients.[72] However, in a Russian population, no significant association between XFS and history of cardiovascular disease was found.[73]

It is interesting to note that even in highly controlled homogenous genetic background and other variables, there is a large heterogeneity of cardiomegaly in dbm mice (Figure 5A). It is also intriguing that the enlarged optic

nerve phenotype in dbm mice also exhibits large heterogeneity. Although we did not observe cataract formation or exfoliation material in dbm mice, which could be attributed by the young age of those mice, because of other findings we believe dbm mice should be further explored as an excellent model to understand both ocular and cardiovascular disorders in XFS patients.

The dbm mice also exhibit other systemic findings commonly observed in XFS patients. Using the Utah database, Wirostko and associates discovered increased risk of XFS in women with POP.[16] As shown in Table 1, we observed 44% rate of POP in dbm mice, females greater than males, and none of the female dbm mice had a history of pregnancy. The average age of detected POP was 12 weeks. One female mouse had POP at 3 weeks of age, and interestingly, that individual died earlier than average. The POP phenotype was well documented in the original report of *Loxl1*$^{-/-}$ mice, and it is correlated with abnormal elastic fibers of pelvic floor.[15] The *Loxl1*$^{-/-}$ mice have since been extensively studied as a model of POP, especially pregnancy-induced POP.[21,74] The earlier onset of POP unrelated to pregnancy in our dbm mice indicate that dbm may be a better model to understand POP in human patients with XFS.

In addition to POP, the Utah database also revealed increased risk of chronic obstructive pulmonary disease in patients with XFS.[18] We observed severe pulmonary emphysema and bronchiectasis in dbm mice, which further supports the utility of this model for human XFS. Last, the association between XFS and retinal vein occlusion has been frequently observed, although the mechanisms remain unknown.[75] We observed striking multifocal leukocytoclastic arteritis in dbm mice. It remains speculative that the arterial wall changes observed in the dbm mice may be present in XFS patients, which may contribute to the higher incidence of retinal vein occlusion.

There are limitations of the dbm model because exfoliation material deposition, elevated IOP and RGC loss, features commonly observed in XFS/XFG patients, were not observed. We speculate this is largely attributed by the young age of those mice as XFS/XFG is an age-related condition in humans. The unique mouse model with microfibril and elastic fiber defects present many other ocular and systemic disorders that are similarly observed in patients with XFS. Although mice differ from humans, the model offers opportunities to investigate XFS pathogenesis.

CREDIT AUTHORSHIP CONTRIBUTION STATEMENT

Rachel W. Kuchtey: Writing – original draft, Visualization, Validation, Supervision, Resources, Project administration, Methodology, Investigation, Funding acquisition, Formal analysis, Data curation, Conceptualization. **Samuel Insignares:** Writing – review & editing, Methodology, Formal analysis, Data curation. **Tzushan S. Yang:** Writing – review & editing, Methodology, Formal analysis, Data curation. **John Kuchtey:** Writing – review & editing, Methodology, Investigation, Formal analysis, Data curation, Conceptualization.

This study was supported by National Eye Institute (NEI) grant EY020894 (R.W.K.), The Glaucoma Foundation (R.W.K.), Vanderbilt Vision Research Center (NEI grant P30EY008126), unrestricted award from Research to Prevent Blindness, Inc, and NCI grant P30CA068485 to the Vanderbilt Translational Pathology Shared Resource. Financial Disclosures: The authors indicate no financial support or conflicts of interest. All authors attest that they meet the current ICMJE criteria for authorship.

REFERENCES

1. Ritch R, Schlötzer-Schrehardt U. Exfoliation syndrome. *Surv Ophthalmol*. 2001;45(4):265–315. doi:10.1016/s0039-6257(00)00196-x.
2. Ritch R, Schlötzer-Schrehardt U, Konstas AGP. Why is glaucoma associated with exfoliation syndrome? *Prog Retin Eye Res*. 2003;22(3):253–275.
3. Gaasterland D, Tanishima T, Kuwabara T. Axoplasmic flow during chronic experimental glaucoma. 1. Light and electron microscopic studies of the monkey optic nervehead during development of glaucomatous cupping. *Invest Ophthalmol Vis Sci*. 1978;17(9):838–846.
4. Quigley HA, Addicks EM. Regional differences in the structure of the lamina cribrosa and their relation to glaucomatous optic nerve damage. *Arch Ophthalmol*. 1981;99(1):137–143.
5. Burgoyne CF, Crawford Downs J, Bellezza AJ, Francis Suh JK, Hart RT. The optic nerve head as a biomechanical structure: a new paradigm for understanding the role of IOP-related stress and strain in the pathophysiology of glaucomatous optic nerve head damage. *Prog Retin Eye Res*. 2005;24(1):39–73. doi:10.1016/j.preteyeres.2004.06.001.
6. Bellezza AJ, Rintalan CJ, Thompson HW, Downs JC, Hart RT, Burgoyne CF. Deformation of the lamina cribrosa and anterior scleral canal wall in early experimental glaucoma. *Invest Ophthalmol Vis Sci*. 2003;44(2):623–637.
7. Sigal IA, Ethier CR. Biomechanics of the optic nerve head. *Exp Eye Res*. 2009;88(4):799–807. doi:10.1016/j.exer.2009.02.003.
8. Quigley H, Anderson DR. The dynamics and location of axonal transport blockade by acute intraocular pressure elevation in primate optic nerve. *Invest Ophthalmol*. 1976;15(8):606–616.
9. Quigley HA, Anderson DR. Distribution of axonal transport blockade by acute intraocular pressure elevation in the primate optic nerve head. *Invest Ophthalmol Vis Sci*. 1977;16(7):640–644.
10. Coudrillier B, Pijanka JK, Jefferys JL, et al. Glaucoma-

related changes in the mechanical properties and collagen micro-architecture of the human sclera. *PloS One*. 2015;10(7):e0131396. doi:10.1371/journal.pone.0131396.
11. Allingham RR, Loftsdottir M, Gottfredsdottir MS, et al. Pseudoexfoliation syndrome in Icelandic families. *Br J Ophthalmol*. 2001;85(6):702–707. doi:10.1136/bjo.85.6.702.
12. Thorleifsson G, Magnusson KP, Sulem P, et al. Common sequence variants in the LOXL1 gene confer susceptibility to exfoliation glaucoma. *Science*. 2007;317(5843):1397–1400. doi:10.1126/science.1146554.
13. Aung T, Ozaki M, Lee MC, et al. Genetic association study of exfoliation syndrome identifies a protective rare variant at LOXL1 and five new susceptibility loci. *Nat Genet*. 2017;49(7):993–1004. doi:10.1038/ng.3875.
14. Mecham RP. Elastin synthesis and fiber assembly. *Ann N Y Acad Sci*. 1991;624:137–146.
15. Liu X, Zhao Y, Gao J, et al. Elastic fiber homeostasis requires lysyl oxidase-like 1 protein. *Nat Genet*. 2004;36(2):178–182. doi:10.1038/ng1297.
16. Wirostko BM, Curtin K, Ritch R, et al. Risk for exfoliation syndrome in women with pelvic organ prolapse: a Utah Project on Exfoliation Syndrome (UPEXS) study. *JAMA Ophthalmol*. 2016;134(11):1255–1262. doi:10.1001/jamaophthalmol.2016.3411.
17. Besch BM, Curtin K, Ritch R, Allingham RR, Wirostko BM. Association of exfoliation syndrome with risk of indirect inguinal hernia: the Utah Project on Exfoliation Syndrome. *JAMA Ophthalmol*. 2018;136(12):1368–1374. doi:10.1001/jamaophthalmol.2018.4157.
18. Taylor SC, Bernhisel AA, Curtin K, Allingham RR, Ritch R, Wirostko BM. Association between chronic obstructive pulmonary disease and exfoliation syndrome: the Utah Project on Exfoliation Syndrome. *Ophthalmol Glaucoma*. 2019;2(1):3–10. doi:10.1016/j.ogla.2018.10.002.
19. Shumway C, Curtin K, Taylor S, Sundar KM, Wirostko BM, Ritch R. Association between obstructive sleep apnea and exfoliation syndrome: the Utah Project on Exfoliation Syndrome. *Ophthalmol Glaucoma*. 2021;4(3):260–267. doi:10.1016/j.ogla.2020.09.016.
20. Wirostko BM, Curtin K, Taylor SC, et al. Risk of atrial fibrillation is increased in patients with exfoliation syndrome: the Utah Project on Exfoliation Syndrome (UPEXS). *Acta Ophthalmol (Copenh)*. 2022;100(4):e1002–e1009. doi:10.1111/aos.15017.
21. Couri BM, Borazjani A, Lenis AT, et al. Validation of genetically matched wild-type strain and lysyl oxidase-like 1 knockout mouse model of pelvic organ prolapse. *Female Pelvic Med Reconstr Surg*. 2014;20(5):287–292. doi:10.1097/SPV.0000000000000104.
22. Pasquale LR, Borrás T, Fingert JH, Wiggs JL, Ritch R. Exfoliation syndrome: assembling the puzzle pieces. *Acta Ophthalmol (Copenh)*. 2016;94(6):e505–e512. doi:10.1111/aos.12918.
23. Aboobakar IF, Johnson WM, Stamer WD, Hauser MA, Allingham RR. Major review: exfoliation syndrome; advances in disease genetics, molecular biology, and epidemiology. *Exp Eye Res*. 2017;154:88–103. doi:10.1016/j.exer.2016.11.011.
24. Topouzis F, Founti P, Yu F, Wilson MR, Coleman AL. Twelve-year incidence and baseline risk factors for pseudoexfoliation: the Thessaloniki Eye Study (an American Ophthalmological Society Thesis). *Am J Ophthalmol*. 2019;206:192–214. doi:10.1016/j.ajo.2019.05.005.
25. Lee VS, Halabi CM, Hoffman EP, et al. Loss of function mutation in *LOX* causes thoracic aortic aneurysm and dissection in humans. *Proc Natl Acad Sci U S A*. 2016;113(31):8759–8764. doi:10.1073/pnas.1601442113.
26. Dietz HC. Marfan Syndrome. In: Pagon RA, Adam MP, Ardinger HH, et al., eds. *GeneReviews(®)*. University of Washington, Seattle; 1993. Accessed April 8, 2017. http://www.ncbi.nlm.nih.gov/books/NBK1335/
27. Bolar N, Van Laer L, Loeys BL. Marfan syndrome: from gene to therapy. *Curr Opin Pediatr*. 2012;24(4):498–504. doi:10.1097/MOP.0b013e3283557d4c.
28. De Paepe A, Devereux RB, Dietz HC, Hennekam RC, Pyeritz RE. Revised diagnostic criteria for the Marfan syndrome. *Am J Med Genet*. 1996;62(4):417–426. doi:10.1002/(SICI)1096-8628(19960424)62:4(417::AID-AJMG15)3.0.CO;2-R.
29. zonule Bassnett SZinn's. *Prog Retin Eye Res*. 2021;82:100902. doi:10.1016/j.preteyeres.2020.100902.
30. De Maria A, Wilmarth PA, David LL, Bassnett S. Proteomic analysis of the bovine and human ciliary zonule. *Invest Ophthalmol Vis Sci*. 2017;58(1):573–585. doi:10.1167/iovs.16-20866.
31. Wu HJ, Hazlewood RJ, Kuchtey J, Kuchtey RW. Enlarged optic nerve axons and reduced visual function in mice with defective microfibrils. *eNeuro*. 2018;5(5). doi:10.1523/ENEURO.0260-18.2018
32. Wareham LK, Kuchtey J, Wu HJ, et al. Lysyl oxidase-like 1 deficiency alters ultrastructural and biomechanical properties of the peripapillary sclera in mice. *Matrix Biol Plus*. 2022;16:100120. doi:10.1016/j.mbplus.2022.100120.
33. Judge DP, Biery NJ, Keene DR, et al. Evidence for a critical contribution of haploinsufficiency in the complex pathogenesis of Marfan syndrome. *J Clin Invest*. 2004;114(2):172–181. doi:10.1172/JCI20641.
34. Ding C, Wang P, Tian N. Effect of general anesthetics on IOP in elevated IOP mouse model. *Exp Eye Res*. 2011;92(6):512–520. doi:10.1016/j.exer.2011.03.016.
35. Dalvin LA, Fautsch MP. Analysis of circadian rhythm gene expression with reference to diurnal pattern of intraocular pressure in mice. *Invest Ophthalmol Vis Sci*. 2015;56(4):2657–2663. doi:10.1167/iovs.15-16449.
36. Wu HJ, Mortlock DP, Kuchtey RW, Kuchtey J. Altered ocular fibrillin microfibril composition in mice with a glaucoma-causing mutation of Adamts10. *Invest Ophthalmol Vis Sci*. 2021;62(10):26. doi:10.1167/iovs.62.10.26.
37. Bermudez MA, Vicente AF, Romero MC, Arcos MD, Abalo JM, Gonzalez F. Time course of cold cataract development in anesthetized mice. *Curr Eye Res*. 2011;36(3):278–284. doi:10.3109/02713683.2010.542868.
38. Koehn D, Meyer KJ, Syed NA, Anderson MG. Ketamine/xylazine-induced corneal damage in mice. *PloS One*. 2015;10(7):e0132804. doi:10.1371/journal.pone.0132804.
39. Sadun AA, Smith LE, Kenyon KR. Paraphenylenediamine: a new method for tracing human visual pathways. *J Neuropathol Exp Neurol*. 1983;42(2):200–206.
40. Zarei K, Scheetz TE, Christopher M, et al. Automated axon counting in rodent optic nerve sections with AxonJ. *Sci Rep*.. 2016;6:26559. doi:10.1038/srep26559.
41. Yuan Y, Schlötzer-Schrehardt U, Ritch R, et al. Transient expression of Wnt5a elicits ocular features of pseudoexfo-

liation syndrome in mice. *PloS One*. 2019;14(3):e0212569. doi:10.1371/journal.pone.0212569.
42. Sultan G, Baudouin C, Auzerie O, et al. Cornea in Marfan disease: Orbscan and in vivo confocal microscopy analysis. *Invest Ophthalmol Vis Sci*. 2002;43(6):1757–1764.
43. Feneck EM, Souza RB, Lewis PN, Hayes S, Pereira LV, Meek KM. Developmental abnormalities in the cornea of a mouse model for Marfan syndrome. *Exp Eye Res*. 2020;194:108001. doi:10.1016/j.exer.2020.108001.
44. Saszik SM, Robson JG, Frishman LJ. The scotopic threshold response of the dark-adapted electroretinogram of the mouse. *J Physiol*. 2002;543(Pt 3):899–916. doi:10.1113/jphysiol.2002.019703.
45. Wu HJ, Kuchtey RW, Kuchtey J. Optic neuropathy associated with TGFβ dysregulation in mice with a glaucoma-causative mutation of Adamts10. *Matrix Biol J Int Soc Matrix Biol*. October 7, 2022 Published online:S0945-053X(22)00123-8. doi:10.1016/j.matbio.2022.10.001.
46. Wu HJ, Hazlewood RJ, Kuchtey J, Kuchtey RW. Enlarged optic nerve axons and reduced visual function in mice with defective microfibrils. *eNeuro*. 2018;5(5). doi:10.1523/ENEURO.0260-18.2018.
47. Pazos M, Yang H, Gardiner SK, et al. Expansions of the neurovascular scleral canal and contained optic nerve occur early in the hypertonic saline rat experimental glaucoma model. *Exp Eye Res*. 2016;145:173–186. doi:10.1016/j.exer.2015.10.014.
48. Cooper ML, Crish SD, Inman DM, Horner PJ, Calkins DJ. Early astrocyte redistribution in the optic nerve precedes axonopathy in the DBA/2J mouse model of glaucoma. *Exp Eye Res*. 2016;150:22–33. doi:10.1016/j.exer.2015.11.016.
49. Liu Y, Schmidt S, Qin X, et al. Lack of association between LOXL1 variants and primary open-angle glaucoma in three different populations. *Invest Ophthalmol Vis Sci*. 2008;49(8):3465–3468. doi:10.1167/iovs.08-1850.
50. Ramirez F, Sakai LY. Biogenesis and function of fibrillin assemblies. *Cell Tissue Res*. 2010;339(1):71–82. doi:10.1007/s00441-009-0822-x.
51. Kielty CM. Fell-Muir Lecture: Fibrillin microfibrils: structural tensometers of elastic tissues? *Int J Exp Pathol*. 2017;98(4):172–190. doi:10.1111/iep.12239.
52. Busnadiego O, Gorbenko Del Blanco D, González-Santamaría J, et al. Elevated expression levels of lysyl oxidases protect against aortic aneurysm progression in Marfan syndrome. *J Mol Cell Cardiol*. 2015;85:48–57. doi:10.1016/j.yjmcc.2015.05.008.
53. Wu HJ, Krystofiak E, Kuchtey J, Kuchtey RW. Enhanced optic nerve expansion and altered ultrastructure of elastic fibers induced by lysyl oxidase inhibition in a mouse model of Marfan syndrome. *Am J Pathol*. March 26, 2024 Published onlineS0002-9440(24)0. doi:10.1016/j.ajpath.2024.03.002.
54. De Maria A, Zientek KD, David LL, et al. Compositional analysis of extracellular aggregates in the eyes of patients with exfoliation syndrome and exfoliation glaucoma. *Invest Ophthalmol Vis Sci*. 2021;62(15):27. doi:10.1167/iovs.62.15.27.
55. Schlötzer-Schrehardt U, Hammer CM, Krysta AW, et al. LOXL1 deficiency in the lamina cribrosa as candidate susceptibility factor for a pseudoexfoliation-specific risk of glaucoma. *Ophthalmology*. 2012;119(9):1832–1843. doi:10.1016/j.ophtha.2012.03.015.
56. Green MC, Sweet HO, Bunker LE. Tight-skin, a new mutation of the mouse causing excessive growth of connective tissue and skeleton. *Am J Pathol*. 1976;82(3):493–512.
57. Chen ZX, Chen TH, Zhang M, et al. Correlation between FBN1 mutations and ocular features with ectopia lentis in the setting of Marfan syndrome and related fibrillinopathies. *Hum Mutat*. 2021;42(12):1637–1647. doi:10.1002/humu.24283.
58. Suwal R, Khadka S, Joshi P. Ocular manifestations and biometrics in Marfan's syndrome from eastern Nepal. *Clin Ophthalmol*. 2020;14:2463–2472. doi:10.2147/OPTH.S269364.
59. White TL, Lewis P, Hayes S, et al. The structural role of elastic fibers in the cornea investigated using a mouse model for Marfan syndrome. *Invest Ophthalmol Vis Sci*. 2017;58(4):2106–2116. doi:10.1167/iovs.16-21358.
60. Iglesias AI, Mishra A, Vitart V, et al. Cross-ancestry genome-wide association analysis of corneal thickness strengthens link between complex and Mendelian eye diseases. *Nat Commun*. 2018;9(1):1864. doi:10.1038/s41467-018-03646-6.
61. Dimasi DP, Burdon KP, Hewitt AW, et al. Candidate gene study to investigate the genetic determinants of normal variation in central corneal thickness. *Mol Vis*.. 2010;16:562–569.
62. Xu X, Zhang X, Cui Y, et al. Three novel variants identified within ECM-related genes in Chinese Han keratoconus patients. *Sci Rep*. 2020;10(1):5844. doi:10.1038/s41598-020-62572-0.
63. Niazi S, Moshirfar M, Alizadeh F, et al. Association of 2 lysyl oxidase gene single nucleotide polymorphisms with keratoconus. *Ophthalmol Sci*. 2023;3(2):100247. doi:10.1016/j.xops.2022.100247.
64. Wiggs JL, Pawlyk B, Connolly E, et al. Disruption of the blood-aqueous barrier and lens abnormalities in mice lacking lysyl oxidase-like 1 (LOXL1). *Invest Ophthalmol Vis Sci*. 2014;55(2):856–864. doi:10.1167/iovs.13-13033.
65. Greene AG, Eivers SB, Dervan EWJ, O'Brien CJ, Wallace DM. Lysyl oxidase like 1: biological roles and regulation. *Exp Eye Res*. 2020;193:107975. doi:10.1016/j.exer.2020.107975.
66. Gordon MO. The Ocular Hypertension Treatment Study: baseline factors that predict the onset of primary open-angle glaucoma. *Arch Ophthalmol*. 2002;120(6):714. doi:10.1001/archopht.120.6.714.
67. Puska P, Vesti E, Tomita G, Ishida K, Raitta C. Optic disc changes in normotensive persons with unilateral exfoliation syndrome: a 3-year follow-up study. *Graefes Arch Clin Exp Ophthalmol*. 1999;237(6):457–462. doi:10.1007/s004170050261.
68. Koz OG, Turkcu MF, Yarangumeli A, Koz C, Kural G. Normotensive glaucoma and risk factors in normotensive eyes with pseudoexfoliation syndrome. *J Glaucoma*. 2009;18(9):684–688. doi:10.1097/IJG.0b013e31819c4311.
69. Schlötzer-Schrehardt UM, Koca MR, Naumann GO. Volkholz H. Pseudoexfoliation syndrome. Ocular manifestation of a systemic disorder? *Arch Ophthalmol*. 1992;110(12):1752–1756. doi:10.1001/archopht.1992.01080240092038.
70. Zehavi-Dorin T, Nahum N, Ben-Artsi E, Levkovitch-Verbin H. Exfoliation syndrome: association with systemic diseases-the Maccabi glaucoma study. *Graefes Arch Clin Exp Ophthalmol*. 2021;259(10):3027–3034. doi:10.1007/s00417-021-05241-w.

71. Mitchell P, Wang JJ, Smith W. Association of pseudoexfoliation syndrome with increased vascular risk. *Am J Ophthalmol*. 1997;124(5):685–687. doi:10.1016/S0002-9394(14)70908-0.
72. Scharfenberg E, Rauscher FG, Meier P, Hasenclever D. Pseudoexfoliation syndrome: analysis of systemic comorbidities of 325 PEX-positive patients compared with 911 PEX-negative patients. *Graefes Arch Clin Exp Ophthalmol*. 2019;257(11):2471–2480. doi:10.1007/s00417-019-04438-4.
73. Bikbov MM, Zainullin RM, Gilmanshin TR, et al. Prevalence and associated factors of pseudoexfoliation in a Russian population: The Ural Eye and Medical Study. *Am J Ophthalmol*. 2020;210:158–166. doi:10.1016/j.ajo.2019.10.003.
74. Liu X, Zhao Y, Pawlyk B, Damaser M, Li T. Failure of elastic fiber homeostasis leads to pelvic floor disorders. *Am J Pathol*. 2006;168(2):519–528. doi:10.2353/ajpath.2006.050399.
75. Ritch R, Prata TS, de Moraes CGV, et al. Association of exfoliation syndrome and central retinal vein occlusion: an ultrastructural analysis. *Acta Ophthalmol (Copenh)*. 2010;88(1):91–95. doi:10.1111/j.1755-3768.2009.01578.x.